國立臺灣大學理學院物理學研究所

碩士論文

Department of Physics

College of Science

National Taiwan University

Master's Thesis

# 藉由熱輔助佔據密度泛函理論對鋰吸附鋸齒型石墨烯奈米帶儲氫性質的研究

# A Thermally-assisted-occupation density functional theory study of hydrogen storage property of Li-adsorbed Zigzag Graphene Nanoribbons

羅義方

Yi-Fang Lo

指導教授: 蔡政達 博士

Advisor: Jeng-Da Chai Ph.D.

中華民國 114 年 7 月

July, 2025

doi:10.6342/NTU202502251

# 國立臺灣大學碩士學位論文
# 口試委員會審定書
## MASTER'S THESIS ACCEPTANCE CERTIFICATE
## NATIONAL TAIWAN UNIVERSITY

藉由熱輔助密度泛函理論對鋰吸附鋸齒型石墨烯奈米帶儲氫性質的研究

A Thermally-assisted-occupation density functional theory study of hydrogen storage property of Li-adsorbed Zigzag Graphene Nanoribbons

本論文係羅義方 R12222021 在國立臺灣大學物理系完成之碩士學位論文，於民國 114 年 7 月 18 日承下列考試委員審查通過及口試及格，特此證明。

The undersigned, appointed by the Department of Physics on 18th July, 2025 have examined a Master's thesis entitled above presented by Yi-Fang Lo R12222021 candidate and hereby certify that it is worthy of acceptance.

口試委員 Oral examination committee:

| | | |
|---|---|---|
| 薛丞宏 | 林倫年 | 趙聖德 |
| （指導教授 Advisor） | | |
| | | |
| | | |



doi:10.6342/NTU202502251

# Acknowledgements

本文能夠順利成篇，首先必需感謝蔡政達老師，若非他的建議以及每週固定的會面討論時間，則本文即使不是不可能產生，也勢必遇到更多的波折、延宕與困難，他在整個研究過程中對我的支持，可以說是在充滿不確定性的研究過程中唯一確定的事情。回顧兩年來的研究生活，從初次接觸密度泛涵理論開始，蔡老師就不厭其煩的解答我在理論上的疑惑，並精準的給予文獻閱讀的建議，而在進入模擬計算時，蔡老師也提供相當多比較容易的系統使我熟悉模擬軟體的操作方式，之後進入研究題目之後遇到的種種問題與困難，蔡老師都願意花時間理解並給予有效的建議或是替代手段，這一切的價值除了引導方向之外，更使我充足的信心完成研究，我相信他對學生的投入毫無疑問位居所有指導教授之前列。

此外，我也要感謝 Dr. Sonai Seenithurai，在整個研究過程中對於我使用 Q-Chem 以及 IQMOL 時相關疑問的解答，Dr. Seenithurai 總是能在我有需要的時候及時回覆我的信件，或甚至是與我實體會面指導我軟體的使用，如果沒有他的提點，我勢必要花上更多的時間查閱手冊並慢慢試錯，他的幫助大大的縮短了我摸索這些軟體的時間。

再來我想要感謝林倫年博士與趙聖德博士兩位委員在口試時給予的建議，雖然礙於時間因素有關於分子動力學模擬以及計算確認 Hessian matrix 的部分無法實現，但是這些質疑讓我更深入的思考本篇研究的侷限性，雖然在畢業之後暫時沒



doi:10.6342/NTU202502251

有繼續深造的打算，但如果將來有機會接觸類似的問題，這些建議都給了我寬闊的視角。

最後，我要感謝我的家人、朋友和其他老師們，你們對本文所提供的幫助或許並不容易直接寫出來，但這絕對不代表它們無關緊要，相反的，他們涉及生活與知識的各個層面，是我成為能完成論文的我無從分割的部分。


doi:10.6342/NTU202502251

# 摘要

本論文以熱輔助佔據密度泛函理論 (thermally-assisted-occupation density functional theory,TAO-DFT)，在廣義密度梯度近似 (generalized gradient approximation,GGA) 加以色散校正 (dispersion correction) 下研究鋰吸附鋸齒型石墨烯奈米帶 (Li-adsorbed zigzag graphene nanoribbons) 之電子性質與儲氫性質。

本文發現在電子性質方面，不論是單純的鋸齒型石墨烯奈米帶或是鋰吸附鋸齒型石墨烯奈米帶，在基本能隙 (Fundamental gap)、對稱馮諾伊曼熵 (symmetrized von Neumann entropy) 以及軌道佔據數目 (orbital occupation number) 的計算結果都顯示此系統具有多重參考性 (multi-reference)，而鋰原子的加入會使此特性更為顯著，這點與之前研究結果類似，也正面說明本文之所以採用熱輔助佔據密度泛函理論而不使用柯恩-沈 (Kohn-Sham) 理論的原因。

在儲氫性質部分，本文發現在固定寬度為兩個苯環的鋰吸附鋸齒型石墨烯奈米帶的長度小於等於三個苯環時，氫氣可以分子的形式在物理吸附其上，且其吸附能量位於或接近理想範圍，此外本所研究的系統在吸附氫氣的重量百分率上亦有優勢。

**關鍵字**：儲氫材料、鋸齒型石墨烯奈米帶、強關聯系統、多重參考、熱輔助佔據密度泛函理論



doi:10.6342/NTU202502251



doi:10.6342/NTU202502251

# Abstract

This thesis employs TAO-DFT (thermally-assisted-occupation density functional theory) under the GGA (generalized gradient approximation ) with dispersion correction to study the hydrogen storage and electronic properties of Li-adsorbed zigzag graphene nanoribbons.

Regarding electronic properties, this study finds that both pristine zigzag graphene nanoribbons and Li-adsorbed zigzag graphene nanoribbons exhibit multi-reference characteristics, as evidenced by calculations of the fundamental gap,orbital occupation number, and symmetrized von Neumann entropy. The addition of lithium atoms further enhances this multi-reference nature. These findings are consistent with some previous studies and substantiate the rationale for using TAO-DFT instead of Kohn-Sham density functional theory.

When it comes to hydrogen storage , this study shows that when the width of Li-adsorbed zigzag graphene nanoribbons is fixed at two benzene rings and the length is



doi:10.6342/NTU202502251

less or than or equal to three benzene rings, hydrogen molecules are able to be physically adsorbed on the nanoribbons, with energy of adsorption falling within or near the ideal range. Furthermore, the studied system demonstrates an advantage in terms of hydrogen adsorption weight percentage.

**Keywords:** hydrogen storage materials, zigzag graphene nanoribbons, multi-reference, strongly correlated system, thermally-assisted-occupation density functional theory



doi:10.6342/NTU202502251

# Contents





doi:10.6342/NTU202502251

doi:10.6342/NTU202502251

# List of Figures





doi:10.6342/NTU202502251

doi:10.6342/NTU202502251

doi:10.6342/NTU202502251



doi:10.6342/NTU202502251

# List of Tables





doi:10.6342/NTU202502251



doi:10.6342/NTU202502251

# Chapter 1 Introduction

Hydrogen possesses a lot of good features that make it possibly a good alternative to fossil fuels. It carries 142 megaJoules of energy per kilogram, which is about two times more efficient than gasoline. In addition, it exists in large quantities on Earth, predominantly in water. What is more important, water vapour is the only product produced when combusted with oxygen. In spite of these ideal features, efficient production, transportation, and storage must be achieved before an economy based on hydrogen power. Among these problems, storing hydrogen has recently been very challenging to the scientific community. One problem of hydrogen is that it is highly flammable and can burst easily when it contacts the environment. Another problem is its large volume. Although storing energy with hydrogen requires little mass, it requires a significant amount of volume if stored in gaseous form. To be specific, a liter of gaseous hydrogen can store only 0.0180 MJ, for liquid hydrogen it can store about 8 MJ, while a liter of gasoline can store 34.8 MJ. Because of these reasons, reversible and safety storage of hydrogen molecules in a compact and lightweight container has been a significant obstacle for an economy based on hydrogen energy. [1–5].

The United States Department of Energy (USDOE) set the ultimate goal of 6.5 wt% concerning the weight-specific hydrogen storage performance of onboard materials for light-duty vehicles[5].Several methods for storing hydrogen have been proposed[1–4].Storage


doi:10.6342/NTU202502251

of physical means where hydrogen is stored inside vessels with huge pressures (e.g., from 350 to 700 bar) , storage of chemical means with which hydrogen is deposited as metal hydrides, cryogenic techniques that involve cooling hydrogen to very low temperatures, typically around 20 K, and adsorption-based method where hydrogen is adsorbed on the surfaces in materials with high surface area. Yet, none succeeded in meeting the USDOE' s combined gravimetric and volumetric storage benchmarks under fast kinetic conditions. However, a number of theoretical analyses have reported materials that may possibly have ideal storage capacities. To adsorb and de-adsorb hydrogen at ambient conditions (1 bar,298K), the ideal adsorption energies of hydrogen molecules should fall between 20 and 40 kJ/mol per $H_2$.[6–8]

To meet the goal aet by USDOE, materials with high surface area such as graphene, metal-organic frameworks (MOFs), and carbon nanotubes have been the focus of extensive research in recent years. However, owing to their weak binding with $H_2$ molecules, these materials can adsorb $H_2$ only at temperatures significantly lower than room temperature. For hydrogen storage at ambient conditions, improving the interaction strength between hydrogen molecules and these materials toward the target range is thus of critical importance.[6–8] To achieve this goal, various innovative methods are being investigated. Common approaches include substitutional doping (e.g., with B or N) and adatom adsorption (e.g., with Li, Al, Ca, or Ti)[3, 9–12]. Among these alternatives, Li adsorption stands out due to its lightweight nature, enabling a high gravimetric storage capacity. Moreover,$H_2$ molecules can be adsorbed by Li strongly via a charge-transfer-induced polarization mechanism, resulting in hydrogen binding energies within the desired range.[2, 13–16] As a result, considerable research has been directed toward exploring hydrogen storage in Li-adsorbed materials.[10, 11, 17–30]


doi:10.6342/NTU202502251

Since the isolation of graphene, a two-dimensional allotrope of carbon with exceptional electrical, mechanical, and thermal properties, considerable attention has been directed toward its nanoscale derivatives. Among these, graphene nanoribbons (GNRs) ,quasi-one-dimensional strips of graphene with widths ranging from several nanometers to tens of nanometers,have emerged as a particularly intriguing class of materials. The reduced dimensionality of GNRs, coupled with their edge morphology and width-dependent electronic behavior, endows them with unique properties that differ markedly from those of pristine graphene.[31–34]

The electronic structure of GNRs is highly sensitive to their edge configuration and width. Notably, armchair-edged GNRs (AGNRs) may exhibit semiconducting behavior with a tunable bandgap, whereas zigzag-edged GNRs (ZGNRs) are often associated with edge-localized states that can give rise to spin-polarized currents and magnetic ordering. These characteristics render GNRs particularly attractive for use in nanoscale transistors, spintronic devices, and quantum computing components.[35–37] GNRs of other kinds of edges are referred as chiral.

In addition to their electronic versatility, GNRs possess high carrier mobility, mechanical robustness, and chemical stability, making them ideal candidates for integration into flexible and miniaturized devices. Recent advances in bottom-up fabrication techniques have further enabled the precise control of GNR width, edge structure, and functionalization, paving the way for systematic exploration of their fundamental properties and technological potential.[38, 39]

In 2016, Seenithurai and Chai published an article discussing the ability for Li-adsorbed n-acenes to store hydrogen molecules and their electronic features.[40]Their results indi-


doi:10.6342/NTU202502251

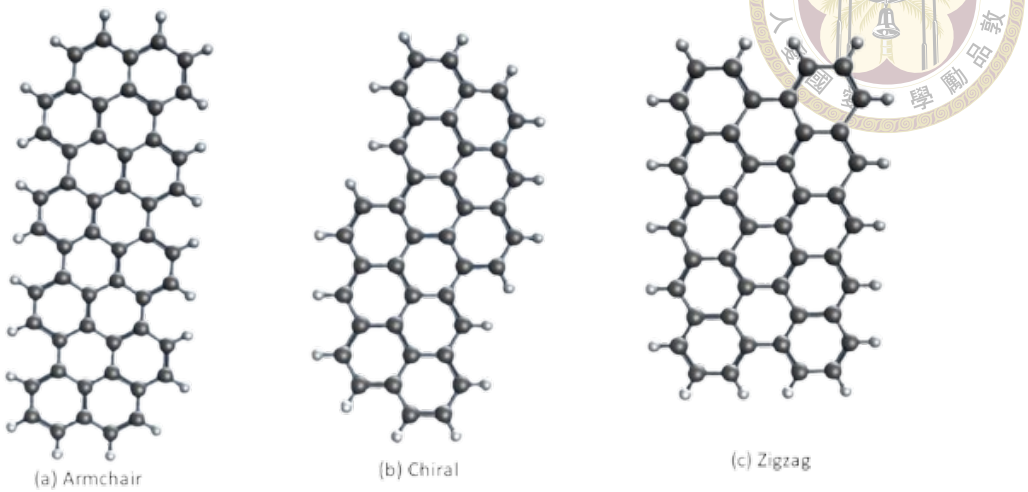


Figure 1.1: Three types of graphene nanoribbons

cate that it is possible for carbon-based material, when adsorbed with a Lithium atom, to adsorb hydrogen molecules reversibly around room temperature. There is also a study on Li-decorated graphene nanoribbons in 2020 by Zheng and others.[41] This thesis serves as a continuation of the above-mentioned works and puts its emphasis on zigzag graphene nanoribbons with a fixed width of two hexagonal carbon rings. For the electronic properties, we follow the analysis scheme used in [40], we will analyze the stability of Lithium atoms, the fundamental gaps, the Symmetrized von Neumann entropy and the occupation numbers. Following the electronic properties, we discuss the hydrogen storage properties. The scheme we employ here is slightly different from that used previously because of the peculiarity of the system, but we try to somehow bridge the two and make comparisons in the discussion section.


doi:10.6342/NTU202502251

# Chapter 2 Theoratical foundation

This chapter discusses the theoretical foundation on which the computational program used in the study is based. I begin by first introducing the density functional theory as a whole. After that, I illustrate the fundamental theorem and algorithm and finally TAO-DFT.

## 2.1 Density functional theory (DFT)

DFT is a method to study properties of large systems and has gained wide popularity among physicists, chemists, and material scientists. In many-body physics, Schrödinger equation, which is a 3N dimensional differential equation,is the fundamental equation that governs the electronic properties. Solving such equation is not feasible and hence a new method must be developed. Before being rigorously proved, people started to wonder if it is possible to get electronic property of the system without looking all 3N degrees of freedom but only the electronic density. In 1927, independently, Thomas and Fermi developed a model now known as Thomas-Fermi model, which gives the kinetic energy of a uniform electron gas in which the mutual interactions are absent and without external potential in terms of an electron density. In 1964, Hohenberg and Kohn rigorously proved that for a system with N electrons and a unique ground state under an external potential,the


doi:10.6342/NTU202502251

electron density is solely specified by the external potential and vice versa (up to a constant). A year later,on the basis of the aforementioned relation, Kohn and Sham invented a self-consistent computational method known as Kohn-Sham DFT (KS-DFT) that can be implemented with computer programs. The core idea behind their method is to reduce an interacting many-body problem in an external potential without time dependence to a non-interacting one in the reference system with an effective external potential. With an assumed self-consistent initial condition, the Kohn-Sham equation is then able to be solved by an iterative process. The Kohn-Sham method makes DFT a practical tool for calculation.

To study a system (i.e. obtain the states and their observables), one begins with the Schrödinger equation:

$$\hat{H}\Psi(\mathbf{x_1},,...,\mathbf{x_N},\mathbf{R_1},...,\mathbf{R_N}) = E\Psi(\mathbf{x_1},...,\mathbf{x_N},\mathbf{R_1},...,\mathbf{R_M}) \tag{2.1}$$

where $\Psi$ is the N electron wave function representing the state,and E is the electronic energy of that state,$x_i \equiv (\mathbf{r}_i, s_i)$ the spatial and spin coordinate of the electron of index i,$R_j$ the spatial coordinate of the nucleus of index j and $\hat{H}$ which includes the kinetic energy of all particles and potential energy among them. To be specific, for a system having N electrons and M nuclei with the charge of the nucleus with index j being $Z_j$ and the mass being $m_j$, all in electronic units. The Hamiltonian operator is

$$\hat{H} = -\sum_{i=1}^{N}\frac{1}{2}\nabla_i^2 - \sum_{j=1}^{M}\frac{1}{2m_j}\nabla_j^2 + \sum_{i'<i}^{N}\frac{1}{|\mathbf{r_{i'}}-\mathbf{r_i}|} + \sum_{j'<j}^{M}\frac{Z_jZ_{j'}}{|\mathbf{R_{j'}}-\mathbf{R_j}|} - \sum_{i=1}^{N}\sum_{j=1}^{M}\frac{Z_j}{|\mathbf{r_i}-\mathbf{R_j}|} \tag{2.2}$$

Since the mass of nuclei are much (about a couple of thousand times) greater than that of an electron, in non-relativistic scenarios, it is appropriate to approximate the nuclei as static.


doi:10.6342/NTU202502251

This is known as the Born-Oppenheimer approximation.Using such an approximation we may drop the $2^{nd}$ term in the Hamiltonian and the forth term is just a constant, which can be shifted to zero. The Hamiltonian then simplifies to

$$\hat{H} = -\sum_{i=1}^{N} \frac{1}{2}\nabla_i^2 - \sum_{i=1}^{N}\sum_{j=1}^{M} \frac{Z_j}{|\mathbf{r_i} - \mathbf{R_j}|} + \sum_{i'<i}^{N} \frac{1}{|\mathbf{r_{i'}} - \mathbf{r_i}|} \tag{2.3}$$

In notations widely used in literature:

$$\hat{H} = \sum_{i=1}^{N} -\frac{1}{2}\nabla_i^2 + \sum_{i=1}^{N} v_{ext}(r_i) + \sum_{i<j}^{N} \frac{1}{\mathbf{r}_{ij}} = \hat{T} + \hat{V}_{ext} + \hat{V}_{ee} \tag{2.4}$$

To simplify the problem, a thing one can do is to consider the electron density, since it is just a function with 3 spatial variables and a spin variable. The relation between electron density and wave function can be easily obtained by the fact that $\Psi^*\Psi$ is a probability density function and is invariant when two of the arguments interchange. It turned out that

$$\rho(\mathbf{x}) = N \int d\mathbf{x_2}...d\mathbf{x_N}\Psi^*(\mathbf{x}, \mathbf{x_2}, ..., \mathbf{x}_N)\Psi(\mathbf{x}, \mathbf{x_2}, ..., \mathbf{x}_N) \tag{2.5}$$

where $d\mathbf{x}_i$ stands for $\sum_{s_i}^{\pm\frac{1}{2}} d\mathbf{r}_i$. From the normalization condition of the wave function, the normalization condition of the density is

$$\int d\mathbf{x}\rho(\mathbf{x}) = N \tag{2.6}$$

which satisfies our intuition.When the system is spin symmetric, it is convenient not to look at the spin degree of freedom but only the spatial part.

$$\rho(\mathbf{r}) = \sum_{s}^{\pm 1/2} \rho(\mathbf{x}) \tag{2.7}$$

From this definition, we can see that for some state $\Psi$, the expectation value of the external


doi:10.6342/NTU202502251

potential :

$$\langle\Psi|V_{ext}|\Psi\rangle = \int d\mathbf{x_1}...d\mathbf{x_N}\Psi^*(\mathbf{x_1},...\mathbf{x_N})V_{ext}(\mathbf{r_1},...,\mathbf{r_N})\Psi(\mathbf{x_1},...\mathbf{x_N}) \tag{2.8}$$

$$= \int d\mathbf{x_1}...d\mathbf{x_N}\sum_{i=1}^{N} v_{ext}(\mathbf{r_i})\Psi^*(\mathbf{x_1},...\mathbf{x_N})\Psi(\mathbf{x_1},...\mathbf{x_N}) \tag{2.9}$$

$$= \sum_{i=1}^{N}\sum_{s_1}^{\pm\frac{1}{2}} \int d\mathbf{r_1}\frac{\rho(\mathbf{r_1},s_1)}{N}v_{ext}(\mathbf{r}_1) = \int d\mathbf{r}\rho(\mathbf{r})v_{ext}(\mathbf{r}) \tag{2.10}$$

The above derivation demonstrated that the potential energy related to the external potential is encodable within a density-dependent functional without any assumption. Suppose that both kinetic energy and inter-electron interaction potential are also functionals of $\rho(\mathbf{r})$. The total energy can be written as

$$E[\rho] = \langle\Psi|\hat{H}|\Psi\rangle = \langle\Psi|\hat{T}+\hat{V}_{ext}+\hat{V}_{ee}|\Psi\rangle \tag{2.11}$$

$$= \langle\Psi|\hat{T}+\hat{V}_{ee}|\Psi\rangle + \int d\mathbf{r}\rho(\mathbf{r})v_{ext}(\mathbf{r}) \tag{2.12}$$

$$= F[\rho] + \int d\mathbf{r}\rho(\mathbf{r})v_{ext}(\mathbf{r}) \tag{2.13}$$

## 2.2 The Hohenberg-Kohn theorems

It was in 1964 that Hohenberg and Kohn [42] proved that for an N-electron system with non-degenerate ground state, there exists a one-to-one (up to a constant) relation linking the ground state density to the external potential. This is known as the First Hohenberg-Kohn theorem and thus justifies the use of electron density as a fundamental variable. To be more specific, since the ground state is acquired by solving the eigenvalue problem of the Hamiltonian, which is determined by the electron number and external potential. By this theorem, having the ground state electron density of a non-degenerate system allows


doi:10.6342/NTU202502251

us to determine the external potential and thus the whole Hamiltonian.

The proof of the First Hohenberg-Kohn theorem goes as follows. Let $V^a_{ext}(\mathbf{r})$ and $V^b_{ext}(\mathbf{r})$ be the external potentials of two N-electron systems. Constructed from these external potentials are the Hamiltonians $\hat{H}^a$ and $\hat{H}^b$ with ground states $\Psi^a(\mathbf{r})$ and $\Psi^b(\mathbf{r})$, respectively. Suppose that the $\Psi^a(\mathbf{r})$ and $\Psi^b(\mathbf{r})$ both lead to $\rho(\mathbf{r})$ Since $\Psi^a(\mathbf{r})$ is the ground state of $\hat{H}^a$, it will not be the ground state of $\hat{H}^b$. So

$$E^b_0 \equiv \langle \Psi^b(\mathbf{r})|H^b(\mathbf{r})|\Psi^b(\mathbf{r})\rangle < \langle \Psi^a(\mathbf{r})|H^b(\mathbf{r})|\Psi^a(\mathbf{r})\rangle \tag{2.14}$$

similarly,

$$E^a_0 \equiv \langle \Psi^a(\mathbf{r})|H^a(\mathbf{r})|\Psi^a(\mathbf{r})\rangle < \langle \Psi^b(\mathbf{r})|H^a(\mathbf{r})|\Psi^b(\mathbf{r})\rangle. \tag{2.15}$$

By linearity of the inner product, we can rewrite:

$$E^b_0 < \langle \Psi^a(\mathbf{r})|\hat{H}^b(\mathbf{r})|\Psi^a(\mathbf{r})\rangle = \langle \Psi^a(\mathbf{r})|\hat{H}^a(\mathbf{r})|\Psi^a(\mathbf{r})\rangle + \langle \Psi^a(\mathbf{r})|\hat{H}^b - \hat{H}^a|\Psi^a(\mathbf{r})\rangle \tag{2.16}$$

This is

$$E^b_0 < \langle \Psi^a(\mathbf{r})|\hat{H}^b(\mathbf{r})|\Psi^a(\mathbf{r})\rangle = E^a_0 + \int d\mathbf{r}\rho(r)[v^b_{ext}(\mathbf{r}) - v^a_{ext}(\mathbf{r})] \tag{2.17}$$

also,

$$E^a_0 < \langle \Psi^b(\mathbf{r})|\hat{H}^a(\mathbf{r})|\Psi^b(\mathbf{r})\rangle = E^b_0 + \int d\mathbf{r}\rho(r)[v^a_{ext}(\mathbf{r}) - v^b_{ext}(\mathbf{r})] \tag{2.18}$$

Adding the above two inequalities, we get

$$E^a_0 + E^b_0 < E^a_0 + E^b_0 \tag{2.19}$$

Which is a contradiction, so our hypothesis that two different potentials can have identical ground state densities is wrong. Hence for a given non-degenerate density, the external


doi:10.6342/NTU202502251

potential is uniquely determined up to a constant. A careful reader may wonder why a constant different in $v^a_{ext}$ and $v^b_{ext}$ leads to no contradiction, this lies in the fact that a constant shift in potential leads only to a phase in the wave function and the density remains invariant.

Proving the one-to-one relation between the ground state density and external potential is not good enough for density functional theory to be applied to real-world problems as it doesn't provide us a way to find such ground states densities. It is the second Hohenberg-Kohn theorem that tells that such ground state densities are also the densities that minimize the energy functionals $E[\rho]$, so that one can get the ground state density via the variation.

From the first Hohenberg-Kohn theorem, there is a one-to-one relation between density and potential[1]. So a trial density $\tilde{\rho}$ has corresponding $\tilde{V}_{ext}$ ,$\tilde{H}$ and also $\tilde{\Psi}$ If the trial density $\tilde{\rho}$ is different from the true ground state density $\rho_0$ than the density functional evaluated with this density is:

$$E[\tilde{\rho}] = \langle\tilde{\Psi}|\hat{H}|\tilde{\Psi}\rangle > \langle\Psi|\hat{H}|\Psi\rangle = E[\rho_0] = E_0 \tag{2.20}$$

which is a consequence directly follows the variational principle of wavefunction. If differentiability of the energy functional is further assumed, we can get the minima by calculus of variations. With the constraint that the density must integrate to total electron

[1] A careful reader may argue that in the proof of first theorem we just discuss densities that is constructed from the non-degenerate ground state wavefunctions of some Hamiltonian and if it is possible that for some density this doesn't hold. The answer is yes, and Levy-Lieb constrained-search formulation was proposed to deal with these cases. But let us assume for now all the trial density comes from the wavefunctions of some non-degenerate ground states. These densities are said to be *v-representable*


doi:10.6342/NTU202502251

number (i.e. $\int d\mathbf{r}\rho(r) = N$), we have

$$\delta\{E[\rho] - \mu\left(\int d\mathbf{r}\rho(\mathbf{r}) - N\right)\} = 0 \tag{2.21}$$

From which the Euler equation is,

$$\mu = \frac{\delta E[\rho]}{\delta\rho(\mathbf{r})} = \frac{\delta F[\rho]}{\delta\rho(\mathbf{r})} + v_{ext}(r) \tag{2.22}$$

The functional $F[\rho]$, being universal and external-potential-independent, is expressed as:

$$F[\rho] = T[\rho] + V_{ee}[\rho],$$

where $T[\rho]$ and $V_{ee}[\rho]$ denote the kinetic and interaction energy functionals, respectively. If such functional form is known and differentiable, then we basically have everything done. However,finding the exact functional form remains challenging and there is no guarantee that such a functional is going to be differentiable. An alternative approach is to introduce a reference system, which I will discuss in the upcoming section.[43]

## 2.3 The Kohn-Sham method

The introduction of a reference system is the key idea behind the Kohn-Sham method. This reference system is assumed to be non-interacting, which means that Schrödinger equation for this system can be solved. Furthermore, it is assumed that the ground state of this reference system will have the same electron density as the real physical system. Introducing such system makes it possible to approximate the kinetic energy functional using the kinetic energy associated with the one-electron solutions of the reference system and the difference between the true physical ground state density and the one evaluated


doi:10.6342/NTU202502251

with the solution from the reference system is known as the *exchange-correlation energy*. With mathematical symbols. The Hamiltonian of the system of reference is of the form:

$$\hat{H}_s = \hat{T}_s + \hat{V}_{eff}$$

where $\hat{V}_{eff}$ does not contain electron-electron interacting term and hence the solutions $\{\phi_i\}$ can be acquired. The kinetic energy density functional is:

$$\hat{T}_s[\rho] = \sum_{i=1}^{N} \langle \phi_i | -\frac{1}{2}\nabla^2 | \phi_i \rangle \tag{2.23}$$

where $\rho$ is assumed to be the ground state density of the system of reference under Kohn-Sham scheme. That is

$$\rho(\mathbf{r}) = \sum_{i=1}^{N} \sum_{s}^{\pm\frac{1}{2}} |\phi_i(\mathbf{r}, s)|^2 \tag{2.24}$$

The effective potential $V_{eff}$ is defined by the potential that the true ground state density is the same as that of the reference system. For the non-interacting reference system, the total energy is:

$$E_s[\rho] = T_s[\rho] + \int d\mathbf{r} v_{eff}(\mathbf{r})\rho(\mathbf{r}) \tag{2.25}$$

From which the Euler equation is

$$\mu_s = v_{eff}(\mathbf{r}) + \frac{\delta T_s[\rho]}{\delta \rho(\mathbf{r})} \tag{2.26}$$

Compare this with the Euler equation of the physical system, with some modification:

$$\mu = \frac{\delta F[\rho]}{\delta \rho(\mathbf{r})} + v_{ext}(\mathbf{r}) = \frac{\delta T_s[\rho]}{\delta \rho(\mathbf{r})} + \frac{\delta E_H[\rho]}{\delta \rho(\mathbf{r})} + \frac{\delta E_{xc}[\rho]}{\delta \rho(\mathbf{r})} + v_{ext}(\mathbf{r}) \tag{2.27}$$


doi:10.6342/NTU202502251

where $T_s[\rho]$ is the same as the one in the non-interacting system, $E_H$ being the simple Coulomb interaction of density, i.e.

$$E_H[\rho] = \frac{1}{2}\int d\mathbf{r_1} d\mathbf{r_2} \frac{\rho(\mathbf{r}_1)\rho(\mathbf{r}_2)}{|\mathbf{r_1} - \mathbf{r_2}|} \tag{2.28}$$

and

$$E_{xc}[\rho] = T[\rho] - T_s[\rho] + V_{ee}[\rho] - E_H[\rho] \tag{2.29}$$

It follows from the definition of $E_H[\rho]$ that

$$\frac{\delta E_H[\rho]}{\delta \rho(\mathbf{r})} = \int d\mathbf{r}' \frac{\rho(\mathbf{r}')}{|\mathbf{r} - \mathbf{r}'|} \tag{2.30}$$

and

$$\frac{\delta E_{xc}[\rho]}{\delta \rho(\mathbf{r})} \equiv v_{xc}(\mathbf{r}) \tag{2.31}$$

So

$$const. = \mu - \mu_s = v_{ext}(\mathbf{r}) - v_{eff}(\mathbf{r}) + \int d\mathbf{r}' \frac{\rho(\mathbf{r}')}{|\mathbf{r} - \mathbf{r}'|} + v_{xc}(\mathbf{r}) \tag{2.32}$$

The effective potential is thus defined

$$v_{eff}(\mathbf{r}) = v_{ext}(\mathbf{r}) + \int d\mathbf{r}' \frac{\rho(\mathbf{r}')}{|\mathbf{r} - \mathbf{r}'|} + v_{xc}(\mathbf{r}) + const. \tag{2.33}$$

The Kohn-Sham method is an iterative method that starts with an initial trial density. From this density, one constructs the effective potential as in (2.33). Than one solves the one particle Schrödinger equation with this effective potential

$$\hat{h}(\mathbf{r})\phi_i(\mathbf{r}) = [-\frac{1}{2}\nabla^2 + v_{eff}(\mathbf{r})]\phi_i(\mathbf{r}) = \epsilon_i \phi_i(\mathbf{r}) \tag{2.34}$$



doi:10.6342/NTU202502251

which is also called the Kohn-Sham equation. The first N solutions of the set $\{\phi_i(r)\}$ will then be used to calculate the new density. If this constructed new density is sufficiently close to the guess, the algorithm terminates and we get the answer. If not, this new density will be used as the new trial density and repeat the process. This is known as the self consistent method. Note that the sum of energies of the first N orbitals is not the physical ground state energy.

$$\sum_{i=1}^{N} \epsilon_i = \sum_{i=1}^{N} \langle \phi_i | -\frac{1}{2}\nabla^2 + \hat{v}_{eff} | \phi_i \rangle \tag{2.35}$$

$$= T_s[\rho] + \int d\mathbf{r}\rho(\mathbf{r})v_{ext}(\mathbf{r}) + \int d\mathbf{r}d\mathbf{r}' \frac{\rho(\mathbf{r})\rho(\mathbf{r}')}{|r-r'|} + \int d\mathbf{r}\rho(\mathbf{r})v_{xc}(\mathbf{r}) \tag{2.36}$$

While the physical ground state energy is:

$$E[\rho] = F[\rho] + \int d\mathbf{r}\rho(\mathbf{r})v_{ext}(\mathbf{r}) = T_s[\rho] + \frac{1}{2}\int d\mathbf{r}d\mathbf{r}' \frac{\rho(\mathbf{r})\rho(\mathbf{r}')}{|r-r'|} + E_{xc}[\rho] + \int d\mathbf{r}\rho(\mathbf{r})v_{ext}(\mathbf{r}) \tag{2.37}$$

So the sum of N orbitals and the true total energy is related by

$$E[\rho] = \sum_{i=1}^{N} \epsilon_i - \frac{1}{2}\int d\mathbf{r}d\mathbf{r}' \frac{\rho(\mathbf{r})\rho(\mathbf{r}')}{|r-r'|} - \int d\mathbf{r}\rho(\mathbf{r})v_{xc}(\mathbf{r}) + E_{xc}[\rho] \tag{2.38}$$

Another thing to note is that for a general solution $\phi_i(\mathbf{r}, s)$, it can be put as

$$\phi_i(\mathbf{r}, s) = \phi_{i\alpha}(\mathbf{r})\alpha(s) + \phi_{i\beta}(\mathbf{r})\beta(s) \tag{2.39}$$

where ,$\alpha(\frac{1}{2}) = \beta(-\frac{1}{2}) = 1$ and $\alpha(-\frac{1}{2}) = \beta(\frac{1}{2}) = 0$ In practical calculations, several assumptions are made to simplify the problem. For a spin-polarized (or spin-unrestricted)calculation, one assumes $\phi_{i\alpha}, \phi_{i\beta}$ be real functions and no mixing. i.e.

$$\phi_i(\mathbf{r}, s) = \phi_{i\alpha}(\mathbf{r})\alpha(s)$$


doi:10.6342/NTU202502251

or

$$\phi_i(\mathbf{r}, s) = \phi_{i\beta}(\mathbf{r})\beta(s)$$

If a system has an even number of electron and the external potential has no spin-dependence, one would often do a spin-unpolarized (or spin-restricted) calculation. The spin-unpolarized calculation takes all the assumptions of spin-polarized calculation, with an additional assumption that

$$\phi_{i\alpha} = \phi_{i\beta}$$

To conclude the section, the invention of Kohn-Sham method reduces the unknown from the universal functional $F[\rho]$ to the exchange-corelation functional $E_{xc}[\rho]$ via the introduction of the approximating N-electron non-interacting reference system and provide an easy iteration process to study the ground state, thus making DFT a popular tool. However, there are still many factors such as the lack of accurate and computationally affordable exchange-correlation functional and the failure to satisfy the assumptions of Kohn-Sham DFT can still cause qualitative error in calculations.[44–47]

## 2.4 Thermally-assisted-occupation density functional theory

In the Kohn-Sham scheme, the density of ground state is assumed to be of the form of equation (2.24). However, high accuracy calculations such as full configuration interaction shows that this assumption fails for some systems. In 2012 Chai proposed a new method known as TAO-DFT (thermally-assisted-occupation density functional theory) to compensate this shortcoming of the conventional KS-DFT while maintaining similar computational cost[48].


doi:10.6342/NTU202502251

In TAO-DFT, the ground state density is assumed to be non-interacting thermal ensemble $v_s$ representable. That is, the density is represented by the ground state density of a reference system consisting of N electrons which are non-interacting and are at the thermal equilibrium with a fictitious electronic temperature $\theta$ when there is a local potential $v_s(\mathbf{r})$. The density is thus of the form:

$$\rho(\mathbf{r}) = \sum_{i=1}^{\infty} f_i |\psi_i(\mathbf{r})|^2 \tag{2.40}$$

with

$$f_i = \frac{1}{1 + \exp[(\epsilon_i - \mu)/\theta]} \tag{2.41}$$

the Fermi-Dirac distribution and $\mu$ determined by

$$\sum_{i=1}^{\infty} f_i = N \tag{2.42}$$

$\psi_i$ being the i-th orbital and $\epsilon_i$ the associated energy. In TAO-DFT, the universal functional is partitioned as

$$F[\rho] = A_s^\theta[\rho] + E_H[\rho] + (V_{ee}[\rho] - E_H[\rho] + T[\rho] - A_s^\theta[\rho]) \tag{2.43}$$

$$= A_s^\theta[\rho] + E_H[\rho] + (V_{ee}[\rho] - E_H[\rho] + T[\rho] - T_s[\rho]) + (T_s[\rho] - A_s^\theta[\rho]) \tag{2.44}$$

$$= A_s^\theta[\rho] + E_H[\rho] + E_{xc}[\rho] + E_\theta[\rho] \tag{2.45}$$

where $A_s^\theta[\rho]$ is the non-interacting $\theta$-temperature kinetic free energy and

$$E^\theta[\rho] \equiv T_s[\rho] - A_s^\theta[\rho] = A_s^{\theta=0}[\rho] - A_s^\theta[\rho] \tag{2.46}$$

One can easily check that for $\theta = 0$ TAO-DFT reduces to KS-DFT. With this new decom-


doi:10.6342/NTU202502251

position of $F[\rho]$ minimizing $E[\rho]$ with constraint leads to

$$\frac{\delta E[\rho]}{\delta \rho} = \mu = \frac{\delta A_s^\theta[\rho]}{\delta \rho} + \int d\mathbf{r}' \frac{\rho(\mathbf{r}')}{|\mathbf{r} - \mathbf{r}'|} + \frac{\delta E_{xc}[\rho]}{\delta \rho} + \frac{\delta E_\theta[\rho]}{\delta \rho} + v_{ext}(\mathbf{r}) \tag{2.47}$$

The direct evaluation of $\frac{\delta A_s^\theta[\rho]}{\delta \rho}$ can be prevented by using Mermin's theorems, which states that the grand-canonical potential $\Omega_s^\theta[\rho]$

$$\Omega_s^\theta[\rho] = A_s^\theta[\rho] + \int d\mathbf{r}\rho(\mathbf{r})[v_s(\mathbf{r}) - \mu_s] \tag{2.48}$$

is minimized. The minimization condition yields the Euler equation

$$\mu_s = \frac{\delta A_s^\theta}{\delta \rho} + v_s(\mathbf{r}) \tag{2.49}$$

along with equation (2.47) we get

$$v_s(\mathbf{r}) = v_{ext}(\mathbf{r}) + \int d\mathbf{r}' \frac{\rho(\mathbf{r}')}{|\mathbf{r} - \mathbf{r}'|} + \frac{\delta E_{xc}[\rho]}{\delta \rho} + \frac{\delta E_\theta[\rho]}{\delta \rho} \tag{2.50}$$

The computation process for TAO-DFT is identical to that of the traditional Kohn-Sham DFT. One begins by an initial guess $\rho_0(\mathbf{r})$ and construct the potential $v_s(\mathbf{r})$ by (2.50). Then one solves the single-particle, non-interacting Schrödinger equation

$$[-\frac{1}{2}\nabla^2 + v_s(\mathbf{r})]\psi_i(\mathbf{r}) = \epsilon_i \psi_i(\mathbf{r})$$

From which one obtains $\{\psi_i\}$ and $\{\epsilon_i\}$. from (2.41) and (2.42) one gets $\mu$ and $\{f_i\}$. Finally one check if $\rho_0(\mathbf{r})$ is close enough to $\rho(\mathbf{r})$ determined by (2.40). If not the process repeats with $\rho(\mathbf{r})$ as the new $\rho_0(\mathbf{r})$. One can express the kinetic free energy $A_s^\theta$ using orbitals and occupation numbers as

$$A_s^\theta = T_s^\theta[\{f_i, \epsilon_i\}] - \frac{\theta}{k_B} S_s^\theta[\{f_i\}] \tag{2.51}$$


doi:10.6342/NTU202502251

where

$$T_s^\theta[\{f_i,\epsilon_i\}] = \sum_{i=1}^{\infty} f_i \int d\mathbf{r}\psi_i^*(-\frac{1}{2}\nabla^2)\psi_i = \sum_{i=1}^{\infty} f_i\epsilon_i - \int d\mathbf{r}v_s(\mathbf{r})\rho(r) \tag{2.52}$$

and the entropy being

$$S_s^\theta[\{f_i\}] = -k_B\sum_{i=1}^{\infty}(1-f_i)\ln(1-f_i) + f_i\ln f_i \tag{2.53}$$

It is thought that the entropy term here plays a significant role in describing the multi-character nature of the system, since when the system is of single-reference nature, one will have $f_i$ being 1 or 0, making the term insignificant. While when the system is of multi-reference character, $f_i$ becomes fractional and this entropy term becomes more important.

## 2.5 Computational detail

A development version of Q-Chem 6.1 is employed for all calculations [49, 50]. Dispersion corrected TAO-DFT with BLYP-D exchange correlation is implemented [51, 52], and the local density approximation density functional with $\theta$ dependency functional $E_\theta^{LDA}$ with the fictitious temperature $\theta$ set to 7 mHartree [48]. In every calculation, we employ the basis set 6−31G* and the fine grid consisting of 75 Euler-Maclaurin radial grid points and 302 Lebedev angular grid points. For weekly interacting systems, to calculate their interaction energies, counterpoise correction process is adopted to reduce the BSSE (basis set superposition errors).


doi:10.6342/NTU202502251

# Chapter 3 Results and discussion

## 3.1 Electronic properties

As the first step we obtain the stable singlet geometry of pristine Zigzag graphene nanoribbon of dimension [2,n](ZGNR[2,n]),where n indicates how many benzene rings are there in direction parallel to the zigzag edge, via geometry optimization with TAO-BLYP-D. At this optimized singlet geometry, we place a Lithium atom at the middle of each of the six-carbon rings and subsequently optimize the geometry again. The position of Lithium atom after optimization is slightly displaced and the structure is then re-optimized. The displaced Lithium atoms turn out to return to approximately the middle of the six-carbon ring, this implies a stable adsorption site for Lithium atom. In this work, ZGNR[2,n] with Lithium atoms adsorbed is written as ZGNR[2,n]-Li, which consists of ZGNR[2,n] and 6n-2 Lithium atoms with the Lithium atoms being adsorbed on the adsorption sites as depicted in Figure 3.1.

Then we evaluate how stably the Lithium atoms are adsorbed via computing the average binding energy of Lithium atoms on ZGNRs, which is:

$$E_b(Li) = (E_{ZGNR[2,n]} + E_{(6n-2)Li} - E_{ZGNR[2,n]-Li})/(6n-2)$$



doi:10.6342/NTU202502251

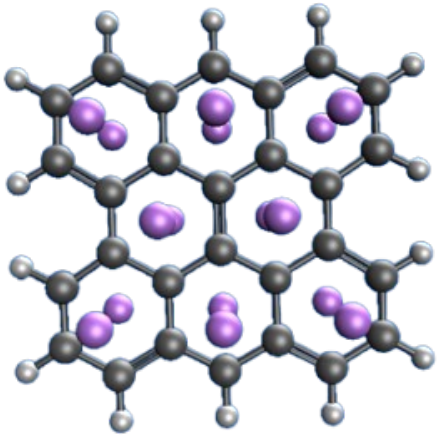

Figure 3.1: Li-adsorbed zigzag graphene nanoribbon

Where $E_{ZGNR[2,n]}$is the total energy of ZGNR[2,n], $E_{(6n-2)Li}$ is the total energy of the 6n-2 Li adatoms on the hexagon sites, and $E_{ZGNR[2,n]-Li}$ is the total energy of Li-adsorbed ZGNR[2,n]. $E_b(Li)$ is then modified for basis set superposition error (BSSE) using a standard counterpoise method, in which the ZGNR[2,n] is considered as the first fragment, and the 6n-2 Li atoms as the second fragment. As expressed in Figure 3.2 ,Li adatoms bind to ZGNR[2,n] strongly with the binding energy range of 75 to 93 kJ/mole for each Lithium. The vertical electron affinity

$$EA_v = E_N - E_{N+1}$$

,ionization potential

$$IP_v = E_{N-1} - E_N$$

, and fundamental gap

$$E_g = IP_v - EA_v = E_{N-1} + E_{N+1} - 2E_N$$

are acquired via several difference of energy calculations, with $E_N$ being the total energy


doi:10.6342/NTU202502251

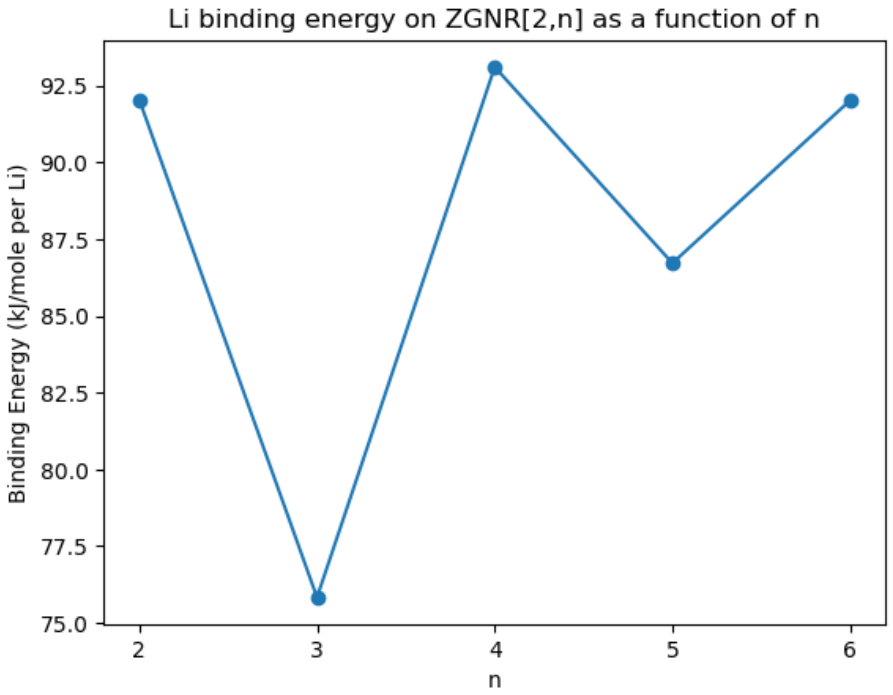


Figure 3.2: Average binding energy of Lithium atoms as a function of n, in kJ/mole

of the neutral system containing N electrons. Here the geometry of the whole systems remains to be that obtained via geometry optimization of the neutral, spin singlet system. When the length n increases, vertical ionization potentials for both pristine ZGNR[2,n] and ZGNR[2,n]-Li tend to decrease.On the other hand,vertical electron affinities tend to increase for both pristine and Li- ZGNR[2,n]. Regarding the fundamental gaps, they decrease monotonically for both pristine ZGNR[2,n] and ZGNR[2,n]-Li.It is also noteworthy that the gap values of Li-adsorbed ZGNR[2,n] (n = 2 – 6) fall within the technologically relevant range of 1 to 3 eV, which is particularly promising for potential applications in nanophotonic devices.

To investigate whether pristine or Li-adsorbed ZGNR[2,n] exhibits multi-reference character, we take a look at the symmetrized von Neumann entropy:

$$S_{vN} = -\frac{1}{2}\sum_{i=1}^{\infty}\{(1-f_i)\ln(1-f_i) + f_i \ln f_i\}$$



doi:10.6342/NTU202502251

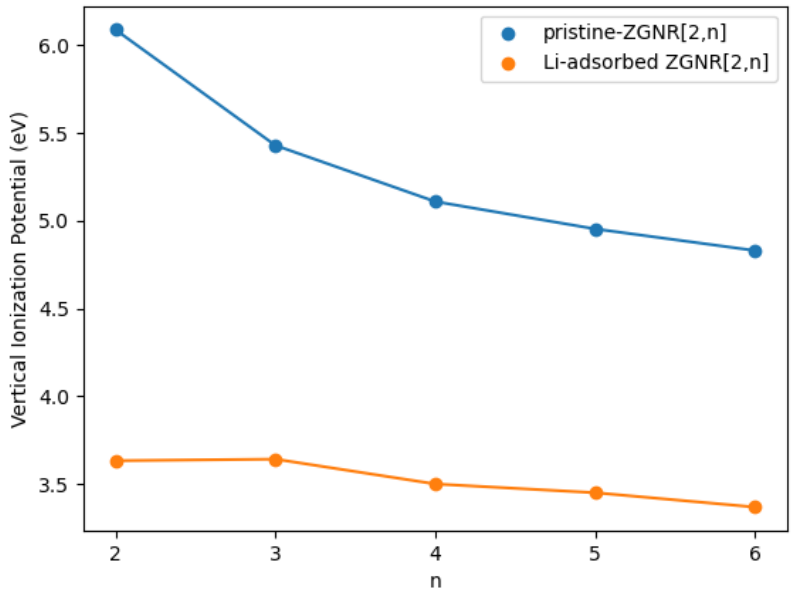


Figure 3.3: Vertical ionization potential as a function of length,in eV

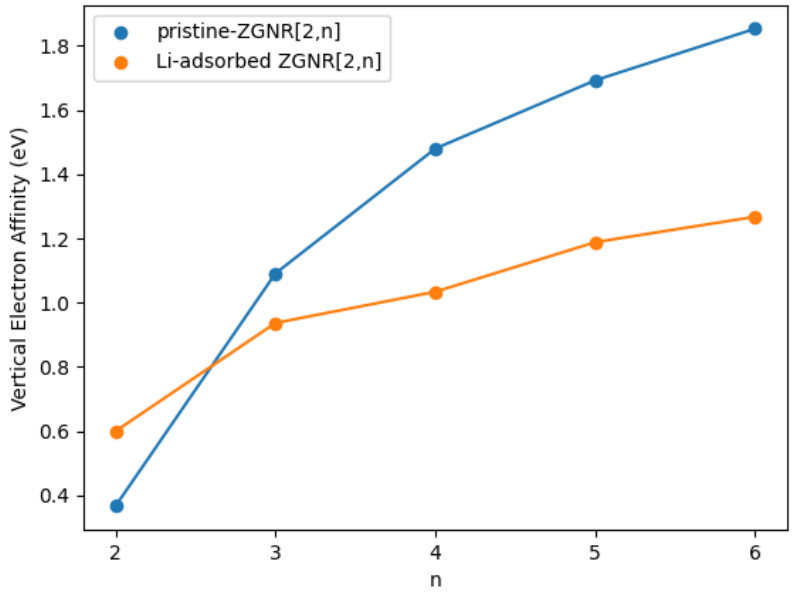


Figure 3.4: Vertical electron affinity as a function of length,in eV



doi:10.6342/NTU202502251

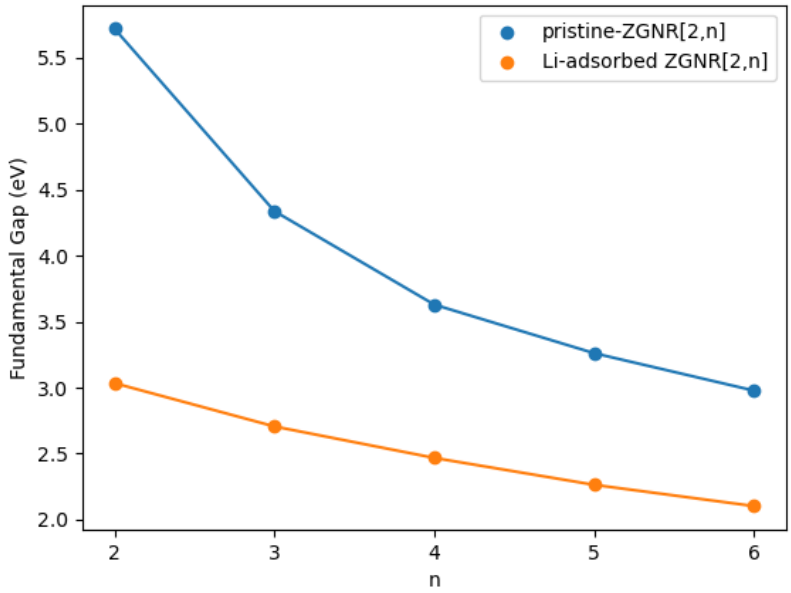


Figure 3.5: Fundamental gap as a function of length,in eV

for the singlet state of pristine/Li-adsorbed ZGNR[2,n] and plot them as a function of length n. In the above equation, $f_i$ is the occupation number of the $i^{th}$ orbital obtained with TAO-BLYP-D, with a value between zero and one, and is about the same as the occupation numbers of the $i^{th}$ natural orbital as pointed out by previous studies[48, 51]. Note that for a system with single reference character, $\{f_i\}$ are very close to either 0 or 1, so the $S_{vN}$ is very close to 0, as the quantity of active orbitals increases, $f_i$ become fractional for these orbitals and $S_{vN}$ increases rapidly. As shown in the following figure for pristine ZGNR[2,n], the Symmetrized von Neumann entropy increases monotonically, these are consistent with the previous TAO-LDA result.[53]

The calculated von Neumann entropy ($S_{vN}$) reveals that Li-adsorbed ZGNR[2,n] systems exhibit a more pronounced multi-reference character than their pristine counterparts for all examined values of n. This observation implies that conventional KS-DFT (Kohn–Sham density functional theory), which relies on standard exchange-correlation functionals, is insufficient for accurately capturing the electronic structure of these systems. How-


doi:10.6342/NTU202502251

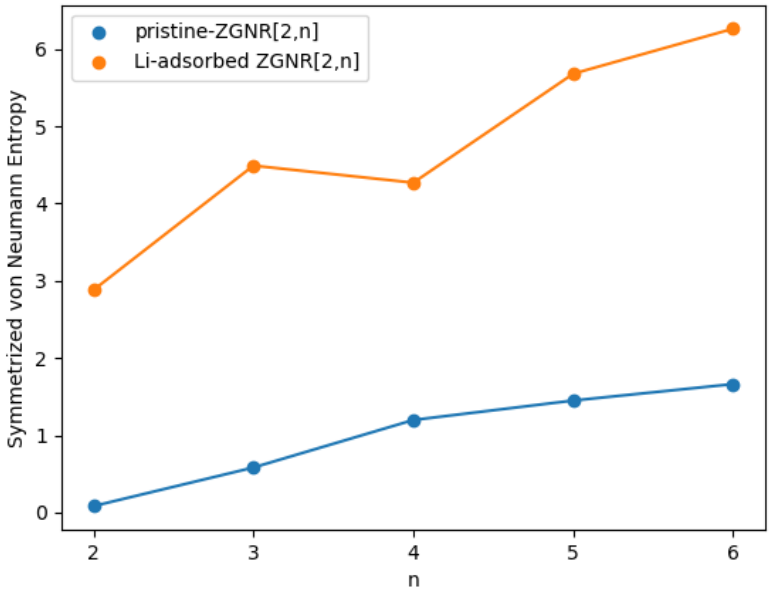


Figure 3.6: Symmetrized von Neumann entropy as a function of length

ever, an increase in $S_{vN}$ alone does not fully elucidate the nature of the underlying electron correlation, as such an increase can result from two distinct scenarios: either most orbital occupation numbers remain close to 0 or 1 with a few approaching 0.5, or a broader set of orbitals attain fractional occupation values that are not necessarily near 0.5. To distinguish between these cases, we examined the orbital occupation numbers for both pristine and Li-adsorbed ZGNR[2,n] systems (n = 2 – 6), considering orbitals ranging from the 10th below the highest occupied molecular orbital (H−10) to the 10th above the lowest unoccupied molecular orbital (L+10). The analysis indicates that both increasing the ribbon length and introducing Li atoms elevate the symmetrized von Neumann entropy, albeit through different mechanisms. While lengthening the system drives more orbitals toward half-occupation, Li adsorption results in a larger number of orbitals with fractional occupation, though not necessarily close to 0.5. Given the prohibitively high computational cost of accurate multi-reference calculations for large ZGNR systems, both pristine and Li-adsorbed, the use of thermally-assisted-occupation DFT (TAO-DFT) is a practical and


doi:10.6342/NTU202502251

justified choice for this study.

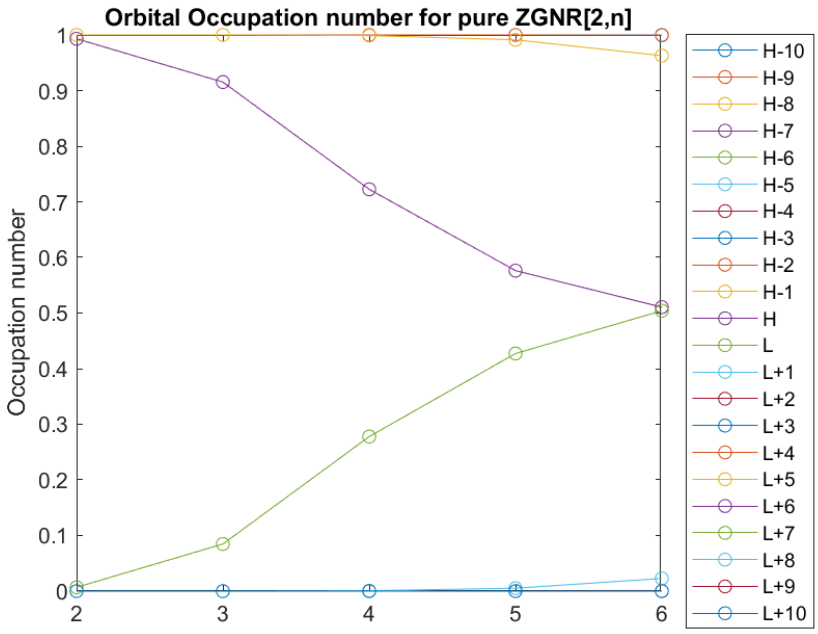


Figure 3.7: Occupation numbers of all orbitals between the 10th orbital below the highest occupied molecular orbital (H-10) and the 10th orbital above the lowest unoccupied molecular orbital(L+10) of ZGNR[2,n](n=2 6)

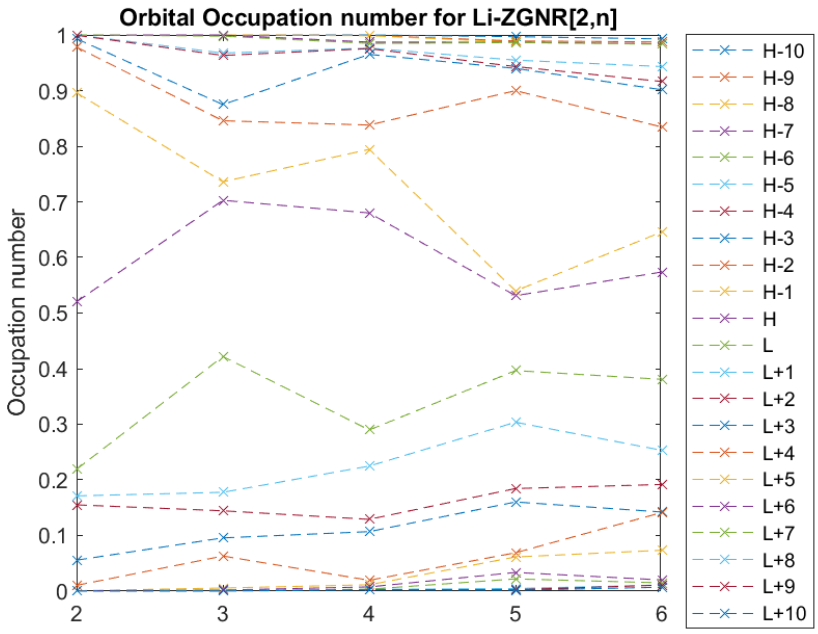


Figure 3.8: Occupation numbers of all orbitals between the 10th orbital below the highest occupied molecular orbital (H-10) and the 10th orbital above the lowest unoccupied molecular orbital(L+10) of Li-ZGNR[2,n](n=2 6)



doi:10.6342/NTU202502251

## 3.2 Hydrogen storage properties

pristine carbon-based materials are found to interact with hydrogen weakly (i.e. mainly by dispersion).Thus they are incapable of storing $H_2$ molecules under ambient conditions. For the same reason, pristine zigzag graphene nanoribbons are unpropitious for ambient hydrogen storage , because of insufficient binding energy. On top of that, the number of hydrogen molecules that every benzene ring can adsorb is constrained by repulsive interactions among them at close proximity. As a consequence, the average binding energy is expected to drop with the increase of hydrogen molecules adsorbed. For these reasons, under ambient conditions, pristine zigzag graphene nanoribbons cannot be efficient hydrogen storage materials. In this thesis, the hydrogen storage properties of Li-adsorbed ZGNR[2,n](n=2,3) are examined. Starting from their ground-state geometries, $x$ hydrogen molecules are first placed at different potential adsorption sites in the neighborhood each Lithium adatom. Geometry optimizations are then carried out to identify the most stable configurations.We focus on the cases where all hydrogen molecules are in their molecular form. The average binding energy of hydrogen, denoted as $E_b(H_2)$, on Li-adsorbed ZGNR[2,n] is calculated using the following definition:

$$E_b(H_2) = (E_{ZGNR[2,n]-Li} + x(6n-2)E_{H_2} - E_{ZGNR[2,n]-Li-x(6n-2)H_2})/[x(6n-2)] \quad (3.1)$$

| | Li-ZGNR[2,2] | Li-ZGNR[2,3] |
|---|---|---|
| $1H_2$ | 29.37 | 30.22 |
| $2H_2$ | 23.25 | 21.07 |
| $3H_2$ | 19.19 | 14.20 |

Table 3.1: Average binding energy of hydrogen molecules, in kJ/mole

Here, $E_{H_2}$ is the energy of a single $H_2$ molecule in vacuum, while $E_{ZGNR[2,n]-Li}$



doi:10.6342/NTU202502251

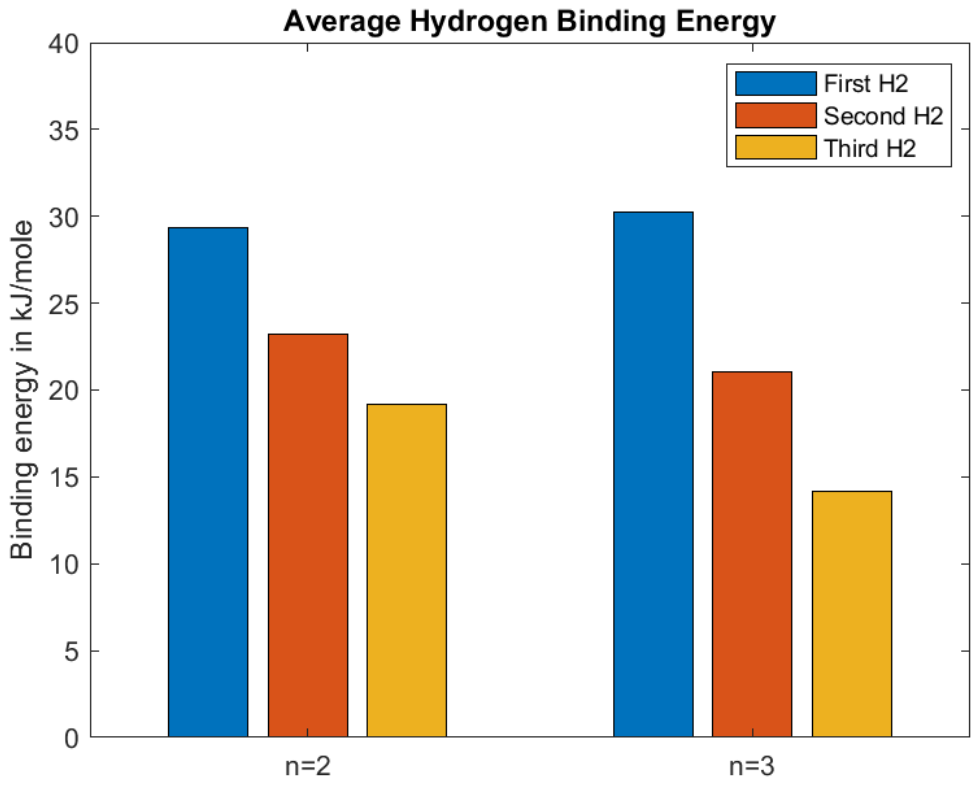


Figure 3.9: Average binding energy of hydrogen molecules, in kJ/mole

corresponds to the total energy of a ZGNR[2,n] structure with Lithium adsorption when $x$ $H_2$ molecules are bound to each Li adatom. The binding energy $E_b(H_2)$ is modified for BSSE via the standard counterpoise scheme. As depicted in the previous table, when x=1, $E_b(H_2)$ is 29 kJ/mole per $H_2$ for n=2 and 30 kJ/mole for n=3. For the case of x=2, $E_b(H_2)$ is 23 kJ/mole per $H_2$ for n=2 and 21 kJ/mole for n=3. These binding energies falls within the ideal energy range. For x=3, however, $E_b(H_2)$ becomes 19 kJ/mole per $H_2$ for n=2 and 13 kJ/mole for n=3, which are below the ideal range.

To evaluate whether the binding energies of each $H_2$ molecule fall within the desirable range for practical hydrogen storage, rather than just considering the average binding energy. We study the binding energy of the y-th $H_2$ molecule. Unlike Li-adsorbed n-acenes, the number of hydrogen atoms that each Li atom can adsorb is different. As a result, we start by checking the final geometry of the system that initially places 3 hydro-


doi:10.6342/NTU202502251

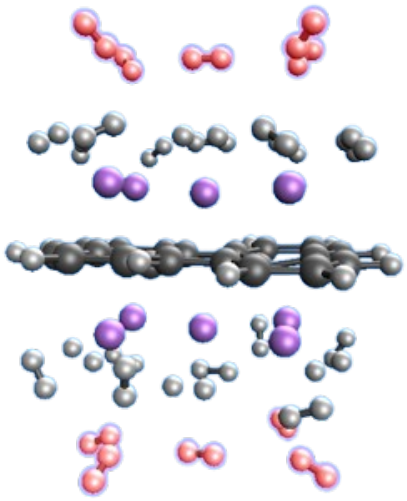

Figure 3.10: The optimized structure containing $30H_2$ adsorbed to Li-adsorbed ZGNR[2,2]. In this figure, hydrogen molecules that are while are of the first type and those in red are of the second type. In this system there is no hydrogen molecules of the third type

gen molecules around each Li atom. From the optimized geometry, we identify different types of hydrogen molecules. The first type of hydrogen molecules are located next to the Li atom. The second type of hydrogen molecules are located a bit farther away from Li atoms. And the last type of hydrogen molecules are those being very far away from the storage system. In this study we will focus on the first two types of hydrogen molecules, in which the second type hydrogen molecules are already weakly adsorbed, justifying our ignorance on the third type. The successive binding energy is defined as, for Li-adsorbed ZGNR[2,2]

$$E_{b,1}(H_2) = (E_{ZGNR[2,2]-Li} + 20E_{H_2} - E_{ZGNR[2,2]-Li-20H_2})/20 \qquad (3.2)$$

$$E_{b,2}(H_2) = (E_{ZGNR[2,2]-Li-20H_2} + 10E_{H_2} - E_{ZGNR[2,2]-Li-30H_2})/10 \qquad (3.3)$$



doi:10.6342/NTU202502251

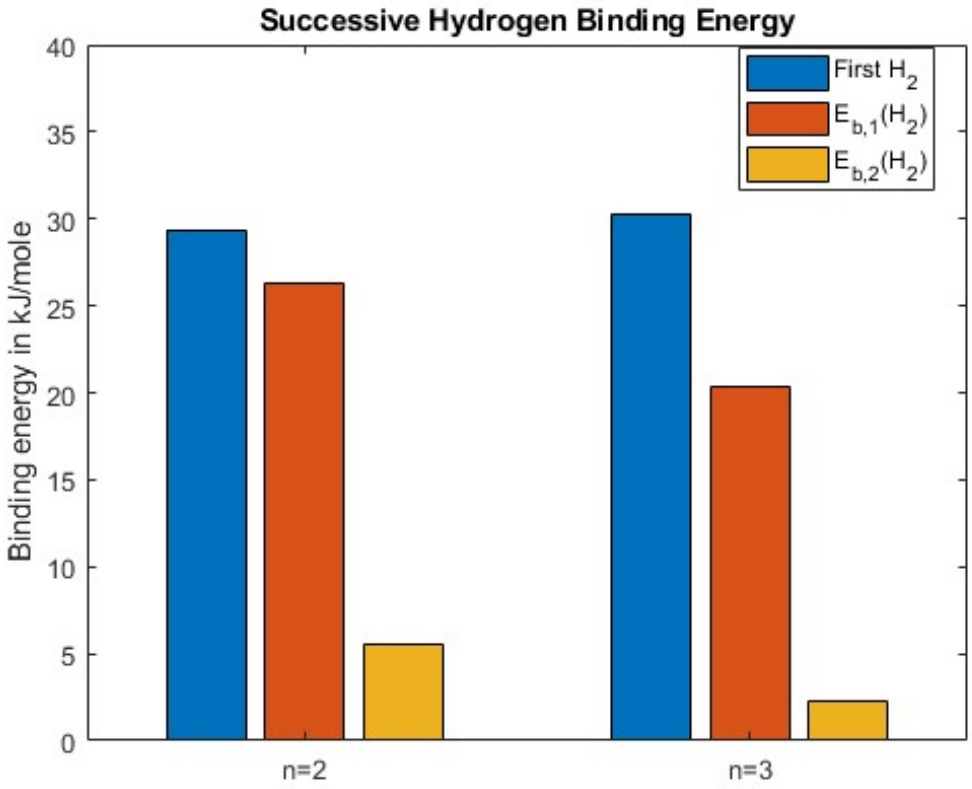


Figure 3.11: Successive binding energy of hydrogen molecules, in kJ/mole

and for Li-adsorbed ZGNR[2,3]

$$E_{b,1}(H_2) = (E_{ZGNR[2,3]-Li} + 22E_{H_2} - E_{ZGNR[2,3]-Li-22H_2})/22 \tag{3.4}$$

$$E_{b,2}(H_2) = (E_{ZGNR[2,3]-Li-22H_2} + 12E_{H_2} - E_{ZGNR[2,3]-Li-34H_2})/12 \tag{3.5}$$

| | Li-ZGNR[2,2] | Li-ZGNR[2,3] |
|---|---|---|
| $E_{b,1}(H_2)$ | 26.24 | 20.30 |
| $E_{b,2}(H_2)$ | 5.58 | 2.27 |

Table 3.2: Successive binding energy of hydrogen molecules, in kJ/mole

The result shows that $E_{b,1}(H_2)$ is 26.24 kJ/mole per $H_2$ for n=2 and 20 kJ/mole per $H_2$ for n=3, $E_{b,2}(H_2)$ is 5.58 kJ/mole per $H_2$ for n=2 and 2.27 kJ/mole per $H_2$ for n=3.


doi:10.6342/NTU202502251

These results show that for hydrogen molecules of the second kind, their interaction with Li-adsorbed ZGNR is weak, and the binding energy is close to that of a dispersion. Thus hydrogen molecules of the second kind is not adsorbed to the system.

By using the van't Hoff equation,[9, 11],we can estimate the temperature at which the adsorbed hydrogen molecules will desorb from the system. Here we use the average binding energy of first hydrogen molecules and $E_{b,1}(H_2)$ for estimation.

$$T_D = \frac{E_b(H_2)}{k_B}\left\{\frac{\Delta S}{R} - \ln\frac{p_0}{p_{eq}}\right\}^{-1} \tag{3.6}$$

Where $E_b(H_2)$ has been defined previously,$\Delta S$ the change in hydrogen from gas to liquid (with value being 13.819R),$p_0$ is the standard atmospheric pressure (1 bar), $p_{eq}$ is the equilibrium pressure and $k_B$, $R$ the Boltzmann and gas constant respectively. As presented in Table 3.3 , the desorption temperature $T_D$ of the adsorbed hydrogen on Li-adsorbed ZGNR[2,n] (n=2,3) is estimated using equation (3.6) at $p_{eq} = 1.5$ bar and 1 bar,respectivel. For the first adsorbed hydrogen molecule, the desorption temperature is about -20 degrees Celsius, and for the average of all adsorbed hydrogen molecules, it becomes about -100 degrees Celsius. With the proper cooling mechanism, Li-adsorbed ZGNR[2,n] can be suitable for hydrogen storage materials near ambient conditions.

As Li-adsorbed ZGNR[2,n] (n=2,3) can bind up to 20 and 22 hydrogen molecules respectively with the average binding energies in the ideal range, the associated hydrogen gravimetric storage capacity $C_g$ is defined as

$$C_g = \frac{mM_{H_2}}{M_{Li-ZGNR[2,n]} + mM_{H_2}} \tag{3.7}$$

where $m$ is the number of hydrogen molecules a system can adsorb,$M_{H_2}$ the mass of a


doi:10.6342/NTU202502251

hydrogen molecule and $M_{Li-ZGNR[2,n]}$ the mass of Li-adsorbed ZGNR[2,n],calculated by using the molecular formula in [53]. As shown in the table. $C_g$ is 11 % for n=2 and 8.7 % for n=3, satisfying the USDOE ultimate target value 6.5 %. However, the what the USDOE target is meant for the whole storage system, which contains not only the storage material but also the enclosing tank, insulation, piping etc. Accordingly, a direct comparison of our calculated result to the USDOE target is not feasible in this case.The actual $C_g$ value will be affected by the design of the entire storage system, so a comparison should only be made after taking all relevant factors into account. However, since the $C_g$ values obtained in this study are higher than the USDOE ultimate target, storage systems utilizing Li-adsorbed ZGNR[2,n] are still likely to serve as high-capacity hydrogen storage materials. On top of the above analysis, let us see how the addition of hydrogen molecules

| n | Binding energy | | $T_D(p_{eq}=1.5)$ | | $T_D(p_{eq}=1)$ | | $C_g$ |
|---|---|---|---|---|---|---|---|
| | $1H_2$ | $E_{b,1}(H_2)$ | $1H_2$ | $E_{b,1}(H_2)$ | $1H_2$ | $E_{b,1}(H_2)$ | |
| 2 | 29.37 | 26.24 | 248 | 222 | 256 | 228 | 11 |
| 3 | 30.22 | 20.30 | 256 | 172 | 263 | 177 | 8.7 |

Table 3.3: Average binding energy, desorption temperature and gravimetric storage capacity. The binding energies are in kJ/mole, temperatures are in K and $C_g$ in percent

affects the electronic properties of the system. To be specific, the occupation number and the symmetrized von Neumann entropy.

| | Li-ZGNR[2,2] | Li-ZGNR[2,3] |
|---|---|---|
| no $H_2$ | 2.88 | 4.49 |
| all $H_2$ of type 1 | 2.16 | 5.06 |
| more $H_2$ | 2.08 | 5.16 |

Table 3.4: Symmetried von Neumann entropy of Li-ZGNR[2,n] and m$H_2$-Li-ZGNR[2,n]

In terms of orbital occupation numbers and symmetrized von Neumann entropy, it can be seen that the adsorption of hydrogen molecules does not change them significantly. That is, the introduction of hydrogen molecules rarely increases or decreases the multi-reference character of the system.


doi:10.6342/NTU202502251

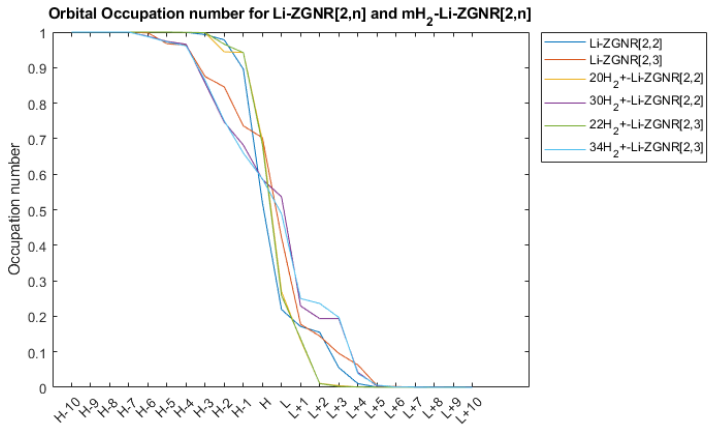


Figure 3.12: Orbital occupation numbers from L-10 to L+10 for Li-ZGNR[2,2] and Li-ZGNR[2,3] with different number of hydrogen molecules adsorbed

As a final part of the analysis, let us take a look on how the addition of hydrogen molecules changes the partial charge of the lithium atoms. The charge we are talking about is the Mulliken atomic charge[54]. As charge can be either positive or negative on each lithium and any non-zero partial charge can polarize the hydrogen molecules, we present here the average absolute value of charge on all lithium atoms in the system.

| | Li-ZGNR[2,2] | Li-ZGNR[2,3] |
|---|---|---|
| no $H_2$ | 0.16 | 0.39 |
| all $H_2$ of type 1 | 0.61 | 0.63 |
| more $H_2$ | 0.73 | 0.74 |

Table 3.5: Average of absolute value of Mulliken charge on Lithium atoms

The result shows that the Mulliken partial charge on lithium atoms increases as the number of hydrogen molecules in the system increases. On top of that, we can see that the difference of partial charge on the lithium atom between the cases when all hydrogen molecules of type one are being adsorbed and the case when no hydrogen molecule is adsorbed is much bigger than that between the cases when more $H_2$ being adsorbed and all hydrogen molecules of type one being adsorbed. In other words, the lithium atoms fail to polarize further when more hydrogen molecules are added to the system, this can possibly set the limit on the binding energy of the hydrogen molecules.


doi:10.6342/NTU202502251

## 3.3 Discussion

It is appropriate to compare our results obtained here to those obtained in the 2016 study on linear Li-adsorbed n-acenes [40] as Li-adsorbed ZGNR[2,n] can be regarded as two parallel n-acene fused together. For electronic properties, both linear n-acenes and ZGNR[2,n] are found to have high multi-reference characters and these characters are further enhanced by the addition of Lithium atoms. The binding energies of Li atoms on both systems are found to be similar.

For hydrogen storage, unlike Li-adsorbed n-acene, the number of hydrogen molecules that each Li adatom can adsorb is different from one to one. It is found that Li adatoms in the center strip of the ribbon adsorb less or even no hydrogen molecules while those on the edge adsorb about one or two hydrogen molecules. Regarding the binding energy, hydrogen molecules are generally adsorbed more strongly on Li-adsorbed n-acene than on Li-adsorbed ZGNR[2,n].This is possibly because of the stronger repulsions among the hydrogen molecules since in Li-adsorbed n-acenes, each benzene ring has at most two neighboring rings, while in Li-adsorbed ZGNR[2,n], each ring can have up to six neighboring rings. As Li atoms are adsorbed at the center of the ring and hydrogen molecules are adsorbed to Li atoms, this will force the hydrogen molecules to be more tightly packed, increasing mutual repulsion [55], hence lowering the binding energy. Unlike n-acenes, the number of hydrogen molecules that each Li atom can adsorb is also different from one to another. This is also very different from n-acene,in which every Li atom in the system can adsorb two hydrogen molecules with the ideal energy range. Besides, during the study, we found that in some of our simulations, hydrogen molecules are torn apart and adsorbed chemically on Li atoms. This occurs more frequently as the system size


doi:10.6342/NTU202502251

gets larger. The occurrence of chemisorption is by far not well understood and was never observed in the n-acene study, but we think these may result from some initial placement of hydrogen molecules that is not physical. It is also worth mentioning that chemisorption occurs only at the Li atoms in the central strip. In Li-adsorbed n-acene systems, the average binding energies are basically around 30-40 kJ/mole per hydrogen molecule, resulting in dissociation temperatures that are close to room temperature or slightly higher than room temperature. On the other hand, for Li-adsorbed ZGNR[2,n], average binding energies are about 20-30 kJ/mole, which correspond to dissociation temperatures that are to some degree lower than room temperature.

Compared to Li-adsorbed n-acenes, Li-adsorbed ZGNR[2,n] have higher gravimetric storage capacity,especially for Li-ZGNR[2,2]. For Li-adsorbed n-acenes, the gravimetric storage capacity is reported to be 9.9 to 10.7 % wt in the study and asymptotes to 11.2 % for $n \to \infty$. For Li-adsorbed ZGNR[2,n], the gravimetric storage capacity is already 11 % wt for n=2 but unfortunately there seems to be no asymptotic result that can be compared.


doi:10.6342/NTU202502251

# Chapter 4 Conclusion

In this work, we examined the hydrogen storage properties of Li-adsorbed zigzag graphene nanoribbons (Li-ZGNR[2,*n*], with *n* = 2, 3) and the electronic properties of Li-adsorbed zigzag graphene nanoribbons (Li-ZGNR[2,*n*], with *n* = 2 - 6) using thermally-assisted-occupation density functional theory (TAO-DFT) with dispersion corrections. Specifically, we analyzed the electronic properties including Li binding energies, vertical electron affinities, ionization potentials, fundamental gaps,symmetrized von Neumann entropy,and orbital occupation numbers. Hydrogen storage descriptors such as the successive and average $H_2$ binding energies, gravimetric storage capacities, and desorption temperatures are also studied. Because of the strong multi-reference character inherent in both pristine and Li-adsorbed ZGNRs, conventional Kohn–Sham DFT with standard exchange–correlation functionals may yield unreliable predictions. In contrast, accurate multi-reference methods such as FCI are computationally infeasible for such large systems, thereby showing the necessity of the employing TAO-DFT.

Our results show that Li-ZGNR[2,2] can accommodate at most 20 $H_2$ molecules and Li-ZGNR[2,3] can accommodate at most 22 $H_2$ molecules with the average energies of binding falling within the ideal range (20–40 kJ/mol per $H_2$). The corresponding temperatures for hydrogen desorption are slightly below room temperature. Regarding the gravimetric storage capacities, they range from 8.7 to 11 %, which exceeds the ultimate


doi:10.6342/NTU202502251

target of 6.5 % set by the USDOE . These findings suggest that Li-adsorbed ZGNR[2,*n*] (n=2,3) systems are promising candidates for high-capacity, reversible hydrogen storage near ambient conditions.

It is also theoretically feasible to decorate both sides of the ZGNR surface with Li atoms. However, experimental implementation may be challenging due to the stacked nature of GNR crystals. As proposed by Deng *et al.*[18], the use of pillared architectures—such as 2,5-dihydrofuran-solvated $Li^+$ cations—to increase the interlayer spacing could potentially allow for sufficient spatial accommodation of both Li adatoms and $H_2$ molecules. Nonetheless, further investigations are warranted to evaluate the properties of such pillared ZGNR systems. Additionally, practical limitations such as Li site occupation by solvent molecules and the reduced stability of Li-doped materials under ambient air or moisture must be addressed through experimental studies.[30]


doi:10.6342/NTU202502251

# References


[1] L. Schlapbach and A. Züttel. Hydrogen-storage materials for mobile applications. Nature, 414:353–358, 2001.

[2] P Jena. Materials for hydrogen storage: past, present, and future. The Journal of Physical Chemistry Letters 2, 206−211, 2011.

[3] N. Park et al. Progress on first-principles-based materials design for hydrogen storage. PNAS, 109:19893–19899, 2012.

[4] A. F. Dalebrook, W. Gan, M. Grasemann, S. Moret, and G. Laurenczy. Hydrogen storage: beyond conventional methods. Chemical Communications, 49:8735–8751, 2013.

[5] U. S. Department of Energy. Target explanation document: onboard hydrogen storage for light-duty fuel cell vehicles. https://energy.gov/eere/fuelcells/hydrogen-storage, 2015. Accessed: June 2025.

[6] R. C. Lochan and M. Head-Gordon. Computational studies of molecular hydrogen binding affinities: the role of dispersion forces, electrostatics, and orbital interactions. Physical Chemistry Chemical Physics, 8:1357–1370, 2006.




doi:10.6342/NTU202502251

[7] S. K. Bhatia and A. L. Myers. Optimum conditions for adsorptive storage. Langmuir, 22:1688–1700, 2006.

[8] K. Sumida et al. Impact of metal and anion substitutions on the hydrogen storage properties of m-btt metal-organic frameworks. Journal of the American Chemical Society, 135:1083–1091, 2013.

[9] E. Durgun, S. Ciraci, and T. Yildirim. Functionalization of carbon-based nanostructures with light transition-metal atoms for hydrogen storage. Physical Review B, 77: 085405, 2008.

[10] S. Seenithurai, R. Kodi Pandyan, S. Vinodh Kumar, C. Saranya, and M. Mahendran. Li-decorated double vacancy graphene for hydrogen storage application: a first principles study. International Journal of Hydrogen Energy, 39:11016–11026, 2014.

[11] N.-X. Qiu, C.-H. Zhang, and Y. Xue. Tuning hydrogen storage in lithium-functionalized BC2N sheets by doping with boron and carbon. ChemPhysChem, 15:3015–3025, 2014.

[12] Sonai Seenithurai and Jeng-Da Chai. Effect of Li termination on the electronic and hydrogen storage properties of linear carbon chains: a TAO-DFT study. Scientific Reports, 7(1):4966, 2017.

[13] J. Niu, B. K. Rao, and P. Jena. Binding of hydrogen molecules by a transition-metal ion. Physical Review Letters, 68:2277–2280, 1992.

[14] J. Niu, B. K. Rao, P. Jena, and M. Manninen. Interaction of H2 and He with metal atoms, clusters, and ions. Physical Review B, 51:4475–4484, 1995.



doi:10.6342/NTU202502251

[15] G. E. Froudakis. Why alkali-metal-doped carbon nanotubes possess high hydrogen uptake. Nano Letters, 1:531–533, 2001.

[16] Rezvan Rahimi and Mohammad Solimannejad. First-principles study of superior hydrogen storage performance of Li-decorated Be2N6 monolayer. International Journal of Hydrogen Energy, 45(38):19465–19478, 2020. ISSN 0360-3199. doi: https://doi.org/10.1016/j.ijhydene.2020.05.047. URL https://www.sciencedirect.com/science/article/pii/S0360319920318243.

[17] P. Chen, X. Wu, J. Lin, and K. L. Tan. High $H_2$ uptake by alkali-doped carbon nanotubes under ambient pressure and moderate temperatures. Science, 285:91–93, 1999.

[18] W.-Q. Deng, X. Xu, and W. A. Goddard. New alkali doped pillared carbon materials designed to achieve practical reversible hydrogen storage for transportation. Physical Review Letters, 92:166103, 2004.

[19] Q. Sun, P. Jena, Q. Wang, and M. Marquez. First-principles study of hydrogen storage on li12c60. Journal of the American Chemical Society, 128:9741–9745, 2006.

[20] A. K. Sabir, W. Lu, C. Roland, and J. Bernholc. Ab initio simulations of H2 in li-doped carbon nanotube systems. Journal of Physics: Condensed Matter, 19:086226, 2007.

[21] Y. Li, G. Zhou, J. Li, B.-L. Gu, and W. Duan. Alkali-metal-doped B80 as high-capacity hydrogen storage media. The Journal of Physical Chemistry C, 112:19268–19271, 2008.

[22] S. Er, G. A. de Wijs, and G. Brocks. Hydrogen storage by polylithiated molecules and nanostructures. The Journal of Physical Chemistry C, 113:8997–9002, 2009.



doi:10.6342/NTU202502251

[23] T. Hussain et al. Ab initio study of lithium-doped graphane for hydrogen storage. EPL, 96:27013, 2011.

[24] S.-H. Huang et al. Lithium-decorated oxidized porous graphene for hydrogen storage by first principles study. Journal of Applied Physics, 112:124312, 2012.

[25] Q. Wang and P. Jena. Density functional theory study of the interaction of hydrogen with li6c60. The Journal of Physical Chemistry Letters, 3:1084–1088, 2012.

[26] P. Li, S. Deng, L. Zhang, G. H. Liu, and J. Yu. Hydrogen storage in lithium-decorated benzene complexes. International Journal of Hydrogen Energy, 37:17153–17157, 2012.

[27] S. J. Kolmann, J. H. D' Arcy, and M. J. T. Jordan. Quantum effects and anharmonicity in the H2-Li+-benzene complex: a model for hydrogen storage materials. The Journal of Chemical Physics, 139:234305, 2013.

[28] Z.-Y. Hu, X. Shao, D. Wang, L.-M. Liu, and J. K. Johnson. A first-principles study of lithium-decorated hybrid boron nitride and graphene domains for hydrogen storage. The Journal of Chemical Physics, 141:084711, 2014.

[29] M. Gaboardi et al. In situ neutron powder diffraction of Li6C60 for hydrogen storage. The Journal of Physical Chemistry C, 119:19715–19721, 2015.

[30] D. Xu, L. Sun, G. Li, J. Shang, R.-X. Yang, and W.-Q. Deng. Methyllithium-doped naphthyl-containing conjugated microporous polymer with enhanced hydrogen storage performance. Chemistry: A European Journal, 22:7944–7949, 2016.

[31] S. Lou, B. Lyu, X. Zhou, et al. Graphene nanoribbons: current status, challenges



doi:10.6342/NTU202502251

and opportunities. Quantum Front, 3:3, 2024. doi: 10.1007/s44214-024-00050-8. URL https://doi.org/10.1007/s44214-024-00050-8.

[32] Yafei Li, Zhen Zhou, Panwen Shen, and Zhongfang Chen. Structural and electronic properties of graphane nanoribbons. The Journal of Physical Chemistry C, 113(33): 15043–15045, 2009.

[33] Oleg V Yazyev. A guide to the design of electronic properties of graphene nanoribbons. Accounts of chemical research, 46(10):2319–2328, 2013.

[34] AV Rozhkov, S Savel' ev, and Franco Nori. Electronic properties of armchair graphene nanoribbons. Physical Review B—Condensed Matter and Materials Physics, 79(12):125420, 2009.

[35] Guo-Ping Guo et al. Quantum computation with graphene nanoribbon. New J. Phys., 11:123005, 2009.

[36] V. Morozov and E. Tretyakov. Spin polarization in graphene nanoribbons functionalized with nitroxide. Journal of Molecular Modeling., 25:58, 2019. doi: 10.1007/s00894-019-3944-4. URL https://doi.org/10.1007/s00894-019-3944-4.

[37] Guo-Hui Ding and Che Ting Chan. Spin-polarized electron transport through graphene nanoribbon with zigzag edges. Journal of Physics: Condensed Matter, 23(20):205304, 2011.

[38] Vivek Saraswat, Robert M. Jacobberger, and Michael S. Arnold. Materials science challenges to graphene nanoribbon electronics. ACS Nano, 15:3674–3708, 2021.

[39] Sandeep Kumar, Surender Pratap, Vipin Kumar, Rajneesh Kumar Mishra, Jin Seog Gwag, and Brahmananda Chakraborty. Electronic, transport, magnetic, and optical



doi:10.6342/NTU202502251

properties of graphene nanoribbons and their optical sensing applications: A comprehensive review. Luminescence, 38(7):909–953, 2023.

[40] S. Seenithurai and J.-D. Chai. Effect of li adsorption on the electronic and hydrogen storage properties of acenes: a dispersion corrected tao-dft study. Scientific Reports, 6:33081, 2016.

[41] Na Zheng, Shulin Yang, Huoxi Xu, Zhigao Lan, Zhao Wang, and Haoshuang Gu. A DFT study of the enhanced hydrogen storage performance of the Li-decorated graphene nanoribbons. Vacuum, 171:109011, 2020.

[42] P. Hohenberg and W. Kohn. Inhomogeneous electron gas. Physical Review, 136: B864–B871, Nov 1964. doi: 10.1103/PhysRev.136.B864. URL https://link.aps.org/doi/10.1103/PhysRev.136.B864.

[43] W. Kohn and L. J. Sham. Self-consistent equations including exchange and correlation effects. Physical Review, 140:A1133–A1138, 1965.

[44] Aron J. Cohen, Paula Mori-Sánchez, and Weitao Yang. Insights into current limitations of density functional theory. Science, 321(5890):792–794, 2008. doi: 10.1126/science.1158722. URL https://www.science.org/doi/abs/10.1126/science.1158722.

[45] Min-Cheol Kim, Eunji Sim, and Kieron Burke. Understanding and reducing errors in density functional calculations. Physical Review Letters, 111:073003, Aug 2013. doi: 10.1103/PhysRevLett.111.073003. URL https://link.aps.org/doi/10.1103/PhysRevLett.111.073003.

[46] Aron J Cohen, Paula Mori-Sánchez, and Weitao Yang. Fractional spins and static



doi:10.6342/NTU202502251

correlation error in density functional theory. The Journal of Chemical Physics, 129 (12), 2008.

[47] Junwei Lucas Bao, Laura Gagliardi, and Donald G. Truhlar. Self-interaction error in density functional theory: An appraisal. The Journal of Physical Chemistry Letters, 9 (9):2353–2358, 2018. doi: 10.1021/acs.jpclett.8b00242. URL https://doi.org/10.1021/acs.jpclett.8b00242. PMID: 29624392.

[48] J.-D. Chai. Density functional theory with fractional orbital occupations. Journal of Chemical Physics, 136:154104, 2012.

[49] Evgeny Epifanovsky, Andrew TB Gilbert, Xintian Feng, Joonho Lee, Yuezhi Mao, Narbe Mardirossian, Pavel Pokhilko, Alec F White, Marc P Coons, Adrian L Dempwolff, et al. Software for the frontiers of quantum chemistry: An overview of developments in the Q-Chem 5 package. The Journal of Chemical Physics, 155(8), 2021.

[50] Anna I Krylov and Peter MW Gill. Q-chem: an engine for innovation. Wiley Interdisciplinary Reviews: Computational Molecular Science, 3(3):317–326, 2013.

[51] J.-D. Chai. Thermally-assisted-occupation density functional theory with generalized-gradient approximations. Journal of Chemical Physics, 140:18A521, 2014.

[52] S. Grimme. Semiempirical gga-type density functional constructed with a long-range dispersion correction. Journal of Computational Chemistry, 27:1787–1799, 2006.

[53] C.-S. Wu and J.-D. Chai. Electronic properties of zigzag graphene nanoribbons studied by tao-dft. Journal of Chemical Theory and Computation, 11:2003–2011, 2015.



doi:10.6342/NTU202502251

[54] Robert S Mulliken. Electronic population analysis on lcao–mo molecular wave functions. i. The Journal of Chemical Physics, 23(10):1833–1840, 1955.

[55] Y. Okamoto and Y. Miyamoto. Ab initio investigation of physisorption of molecular hydrogen on planar and curved graphenes. Journal of Physical Chemistry B, 105: 3470–3474, 2001.



doi:10.6342/NTU202502251



doi:10.6342/NTU202502251

# Appendix A — Figures of real-space representation of HOMOs and LUMOs for the lowest singlet states of pristine and Li-adsorbed ZGNR calculated using spin restricted TAO-BLYP-D ($\theta = 7$mHartree) at isovalue =0.002eV/Å

## A.1 pristine Zigzag graphene nanoribbons [2,n]

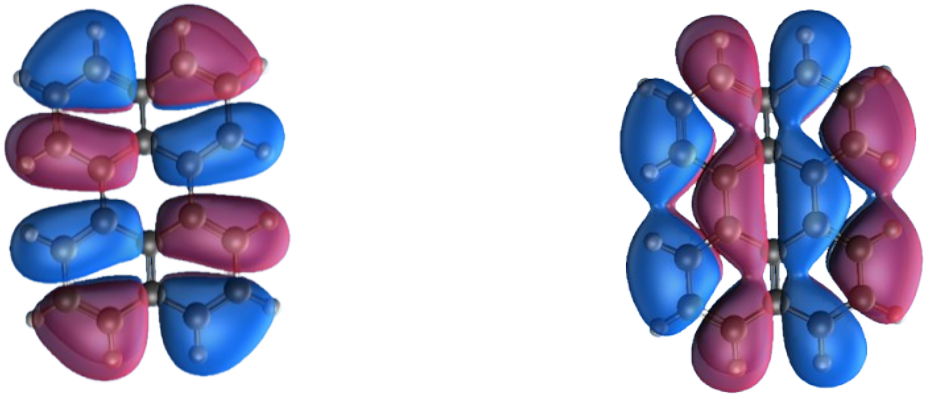

(0.99310) (0.00690)

Figure A.1: Real-space representation of HOMO (left) and LUMO (right) for the singlet state of pristine ZGNR[2,2] with their occupation number 0.99310 and 0.00690.



doi:10.6342/NTU202502251

(0.91526) (0.08475)

Figure A.2: Real-space representation of HOMO (left) and LUMO (right) for the singlet state of pristine ZGNR[2,3] with their occupation number 0.91526 and 0.08475

(0.72246) (0.27791)

Figure A.3: Real-space representation of HOMO (left) and LUMO (right) for the singlet state of pristine ZGNR[2,4] with their occupation number 0.72246 and 0.27791

(0.99994) (0.91526)

Figure A.4: Real-space representation of HOMO (left) and LUMO (right) for the singlet state of pristine ZGNR[2,5] with their occupation number 0.576264 and 0.42726



doi:10.6342/NTU202502251

(0.99994) (0.91526)

Figure A.5: Real-space representation of HOMO (left) and LUMO (right) for the singlet state of pristine ZGNR[2,6] with their occupation number 0.51060 and 0.50413

## A.2 Li-adsorbed Zigzag graphene nanoribbons [2,n]

(0.52016) (0.21912)

Figure A.6: Real-space representation of HOMO (left) and LUMO (right) for the singlet state of Li-ZGNR[2,2] with their occupation number 0.52016 and 0.21912

(0.70266) (0.42173)

Figure A.7: Real-space representation of HOMO (left) and LUMO (right) for the singlet state of Li-ZGNR[2,3] with their occupation number 0.70266 and 0.42173



doi:10.6342/NTU202502251

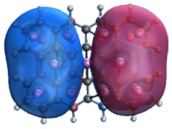

(0.67990)

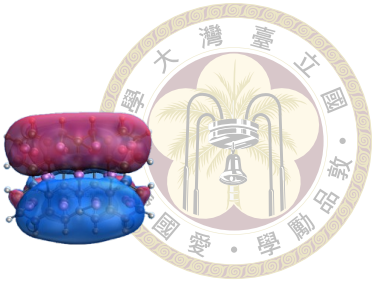

(0.28979)

Figure A.8: Real-space representation of HOMO (left) and LUMO (right) for the singlet state of Li-ZGNR[2,4] with their occupation number 0.67990 and 0.28979

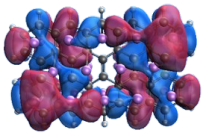

(0.53120)

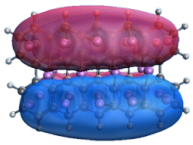

(0.39654)

Figure A.9: Real-space representation of HOMO (left) and LUMO (right) for the singlet state of Li-ZGNR[2,5] with their occupation number 0.53120 and 0.39654

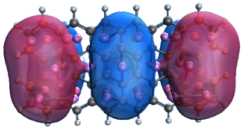

(0.57376)

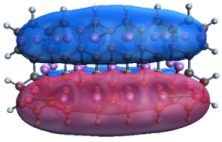

(0.38082)

Figure A.10: Real-space representation of HOMO (left) and LUMO (right) for the singlet state of Li-ZGNR[2,6] with their occupation number 0.57376 and 0.38082



doi:10.6342/NTU202502251



doi:10.6342/NTU202502251

# Appendix B — Figures of optimized geometries of Li-adsrobed ZGNR[2,n] (n=2,3) with various numbers of hydrogen molecules adsorbed

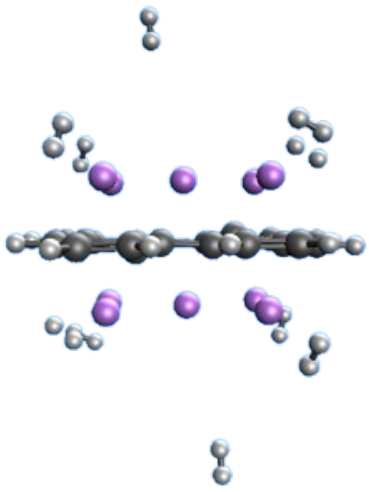

Figure B.11: Optimized geometries of Li-adsrobed ZGNR[2,2] with 10 hydrogen molecules adsorbed



doi:10.6342/NTU202502251

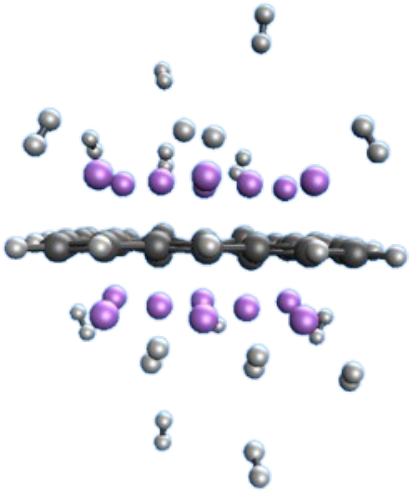

Figure B.12: Optimized geometries of Li-adsrobed ZGNR[2,3] with 16 hydrogen molecules adsorbed

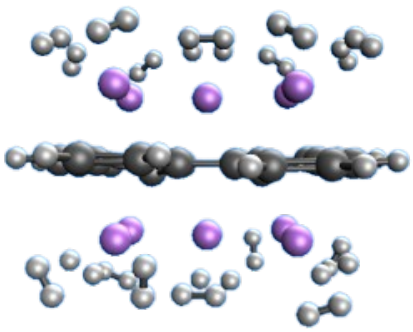

Figure B.13: Optimized geometries of Li-adsrobed ZGNR[2,2] with 20 hydrogen molecules adsorbed



doi:10.6342/NTU202502251

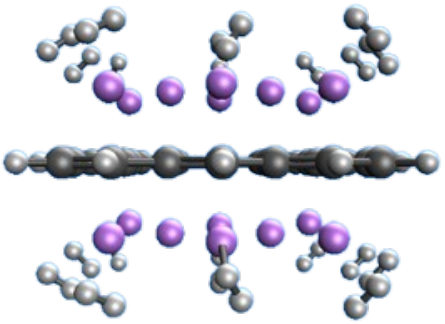

Figure B.14: Optimized geometries of Li-adsrobed ZGNR[2,3] with 22 hydrogen molecules adsorbed

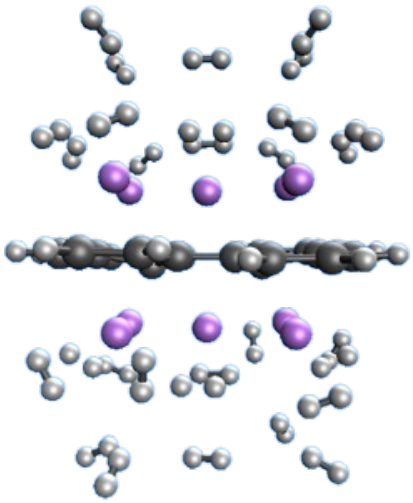

Figure B.15: Optimized geometries of Li-adsrobed ZGNR[2,2] with 30 hydrogen molecules adsorbed



doi:10.6342/NTU202502251

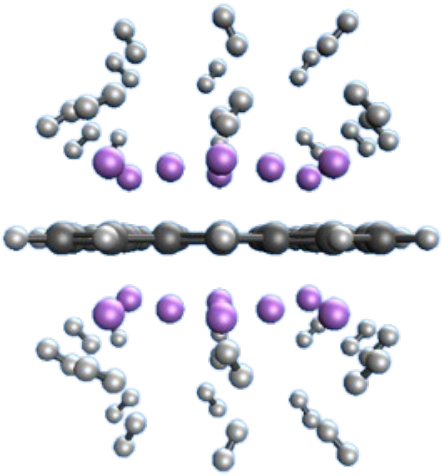

Figure B.16: Optimized geometries of Li-adsrobed ZGNR[2,3] with 34 hydrogen molecules adsorbed



doi:10.6342/NTU202502251